



Operation modes of the helium dielectric barrier discharge for soft ionization

S. Müller^a, T. Krähling^a, D. Veza^b, V. Horvatic^c, C. Vadla^c, J. Franzke^{a,*}

^a ISAS—Leibniz Institut für analytische Wissenschaften, Otto-Hahn-Straße 6b, 44227 Dortmund, Germany

^b Department of Physics, Faculty of Science, University of Zagreb, Bijenicka 32, 10000 Zagreb, Croatia

^c Institute of Physics, Bijenicka 46, 10000 Zagreb, Croatia

ARTICLE INFO

Article history:

Received 25 September 2012

Accepted 10 April 2013

Available online 30 April 2013

Keywords:

Soft ionization

Dielectric barrier discharge

Discharge modes

Homogeneous discharge

Filamentary discharge

ABSTRACT

Among different applications of dielectric barrier discharge (DBD) plasma, the soft ionization ability is certainly one of the most interesting. In this paper the helium plasma jet, produced by a capillary DBD, penetrating in the ambient atmosphere, has been spectroscopically investigated in dependence on applied voltage and helium flow. It was found that the change of the applied voltage leads to different discharge modes. Based on the measurements of the emission spectra of atomic He and N_2^+ and N_2 molecules in the capillary and in the plasma jet with high spatial resolution, it can be assessed in which mode, i.e. under which conditions the plasma jet is expected to be most effective for soft ionization of molecules.

© 2013 Elsevier B.V. All rights reserved.

1. Introduction

In the last years dielectric barrier discharges (DBD) were applied in different fields of analytical chemistry. DBDs are used for the detection of atomic analytes because they are simple and inexpensive and because of their potential for portable detection in real time. Attention has been focused on the application of these plasmas as ambient desorption–ionization (ADI) sources, for the detection of molecular species, capable of producing rapid analytical results with little or no sample preparation [1–7].

Studies have also been conducted on the use of helium-DBDs as ionization sources in ion mobility spectrometry (IMS) and for liquid chromatography/mass spectrometry [8–11].

The ionization mechanisms for He-DBDs used as ambient ionization sources are not completely understood. In some cases, analyte ionization is thought to be the result of charge transfer (CT) from atmospheric nitrogen, or proton transfer from atmospheric water due to an atmospheric-pressure chemical ionization (APCI) process [1,2,12]. Nevertheless, the APCI process begins with the ionization of N_2 [13]. In helium-based atmospheric-pressure plasmas, the ionization of N_2 has also been attributed to Penning ionization (PI) by helium metastable atoms (He^M) [14–17].

Chan et al. have recently published a study of the low-temperature plasma (LTP) in which they present detailed analysis of the emission measurements of excited He and N_2^+ [18]. Other publications have ascribed a major role to He_2^+ in the ionization of atmospheric nitrogen [18,19].

Regardless of the specific ionization mechanism, He^M atoms play a central role, either directly as reagents, or indirectly as precursors for other highly excited helium species. Unfortunately, little research has been done to correlate He^M densities with the performance of helium-based sources.

Our previously performed spatially resolved spectroscopic measurements on a dielectric barrier discharge plasma jet provided additional insight into the relevant excitation energy processes leading to the pronounced ionization of water in air and the subsequent protonation of organic molecules for soft ionization [20]. Intensity distributions in the plasma jet of some relevant atomic emission lines (He 706 nm), and characteristic molecular bands (N_2 380 nm and N_2^+ 391 nm) of the dominant species involved in the energy transfer process have been presented. The plasma jet, which penetrates from the nozzle of the capillary DBD into the atmosphere, possesses strongly non-homogeneous distributions of the ground-state particles. However, the jet is axially symmetric and its non-homogeneity along the axis of penetration is well defined. By combining experimental findings with time-resolved measurements on a helium DBD plasma jet reported by Xiong et al. [21], it can be argued that the main excitation path leading to protonation of water in helium plasma jet penetrating in the air atmosphere starts with collisions between helium metastable atoms and nitrogen molecules in the air. Finally, we agree with Xiong et al. [21] that Penning ionization of nitrogen molecules and subsequent energy transfer to the water molecules are the processes leading to an efficient water ionization and protonation.

Most of the before-mentioned papers dealt with DBDs, but all of them were different in physical properties defined by geometry and power consumption. One of the definitions of a dielectric barrier discharge is that minimum one dielectric layer has to exist between the

* Corresponding author.

E-mail address: joachim.franzke@isas.de (J. Franzke).

electrodes. For example, the DBD called LTP probes, are built up with one electrode surrounding a capillary and the other one inside the capillary, i.e. with only *one* dielectric layer between the electrodes. The dielectric barrier discharges used for IMS and for liquid chromatography/mass spectrometry have a capillary with substantially smaller inner diameter than the latter, which requires geometry with two electrode rings around the capillary. Therefore they have *two* dielectric layers. The properties of these two types of discharges might be very different.

Usually, this kind of DBD can be used for soft ionization when the analyte passes the plasma jet or when analytes will be desorbed from a non-conductive layer. One good example, in which depth profiling of nanometer coatings was accomplished by a low temperature plasma probe [22] (here with two electrodes around the capillary) will demonstrate that. Here, a much higher energy must be applied on the surface than in the case of a desorption procedure. This might be due to the fact that the conductive surface shortcuts the second dielectric and forms another direct electrode. Hence, this dielectric barrier discharge has completely different physical properties than the one used for desorption.

Even small changes of the flow rate or the applied voltage, for instance, can influence the dielectric barrier discharge concerning its ability to accomplish soft ionization. In the present publication spatially dependent spectra measured with a better resolution than previously, for different modes observed in DBD burning in helium are presented. These modes can be set by tuning the applied voltage. A clear separation of the N_2^+ and the N_2 spatial distribution maxima was observed, reflecting the temporal sequence of their production.

2. Experimental arrangement

The experimental arrangement is shown in Fig. 1. The plasma jet was generated by a dielectric barrier discharge, constructed using a 30 mm long glass capillary having an outer diameter of 1.0 mm and an inner diameter of 500 μm . One end of the capillary was the gas inlet and the other one is left in ambient air. Two electrodes surrounding the capillary were 1 mm wide and separated by 10 mm. The distance from the capillary orifice to the first electrode (the anode) was approximately 2 mm.

A Teflon ring was placed in the middle between the electrodes in order to prevent the possible direct discharge in the air at the highest voltages. The emission signals were checked outside the capillary, and it was proven, that there was no discharge forming in the air outside the capillary.

The plasma jet was obtained using He as working gas, which was provided with a gas flow-rate of 600 ml min^{-1} . The electrodes were

connected to a home built high voltage plasma generator [23]. The voltage applied to the electrodes was modulated by rectangular pulses (frequency: 21.5 kHz) provided by a function generator.

The corresponding peak voltage values for stable plasma operation were between 3.5 and 6.5 kV at 21.5 kHz. The DBD was mounted on a micrometer stage enabling translation along its axis.

The electrode–capillary contact is critical for durability and reproducibility of DBD operation. In our present electrode design the DBD exhibited very high stability and could be operated and repeatedly ignited without deterioration in metal–quartz contact for more than one month. For monitoring the discharge current and voltage an oscilloscope (HAMEG HM 203-6) was used. The current was monitored by measuring the voltage drop U_1 over the resistor $R_1 = 1 \Omega$ connected in series with the DBD, while the applied high voltage was represented by the voltage U_2 measured by a potential divider constituting of the resistors $R_2 = 1 \text{ M}\Omega$ and $R_3 = 100 \text{ M}\Omega$.

The distributions of excited He, N_2 and N_2^+ were monitored by measuring the intensity distributions of the He 388 nm line and the molecular bands with maxima at 380 nm and 391 nm, henceforth referred to as N_2 380 nm and N_2^+ 391 band, respectively. The relevant transitions and typical spectra are shown in Fig. 2. The light emerging from the discharge in the capillary or from the jet was observed at right angles with respect to the discharge axis and imaged with a lens ($f = 10 \text{ cm}$, imaging ratio: 1:1) onto the entrance slit (slit width: 40 μm , slit height: 0.5 mm) of 1-m McPherson monochromator (grating: 1200 grooves/mm). The spectral intensities were measured in the second order of the grating dispersion (spectral resolution: 0.025 nm) using an EMI S-11 photomultiplier. The multiplier current was measured by picoammeter (Keithley 4685) and stored on a laboratory PC. In this manner, the transient line intensities occurring within the period of time of the plasma duration were averaged and recorded as continuous spectra.

3. Measurements and results

3.1. Discharge modes

The appearance of different DBD modes under conditions of the present experiment is illustrated in Figs. 3 and 4, where the photographs of the plasma and corresponding discharge voltage and current signals are shown. Here, the applied He flow was 500 ml/min. The DBD starts to burn at 3 kV and the plasma is visible in the capillary between the electrodes and outside of the capillary in the form of a relatively long jet (see upper part of Fig. 3). The brightness of the capillary discharge and the plasma jet as well as the jet length rises continuously with increasing voltage up to approximately 4 kV. With a further increase of the voltage, the brightness of the plasma in the capillary continuously

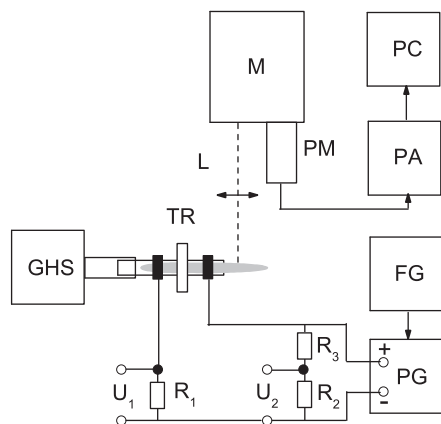


Fig. 1. Experimental arrangement: GHS: gas-handling system, C: cathode, TR: Teflon ring, A: anode, PJ: plasma jet, R_1 : 1 Ω resistor, R_2 : 1 $\text{M}\Omega$ resistor, R_3 : 100 $\text{M}\Omega$ resistor, U_1 and U_2 : voltage signals measured by an oscilloscope, PG: plasma generator, FG: function generator, L: imaging lens, M: monochromator, PM: photomultiplier, PA: pA-meter, PC: personal computer.

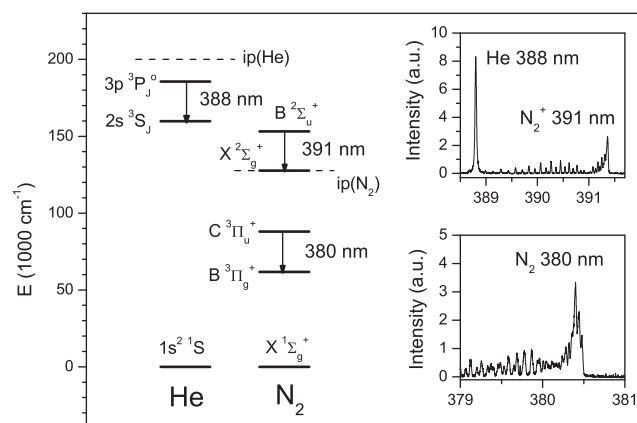


Fig. 2. Simplified term diagrams of He and N_2 with relevant transitions. Insets: typical measured spectra.

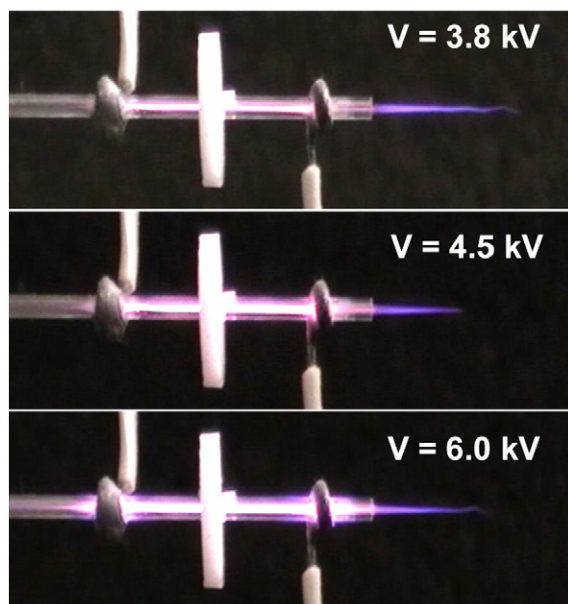


Fig. 3. Photographs of the plasma operating at three representative applied voltages. See further explanation in text.

rises up and starts to extend in the region behind the cathode in the direction to the gas supply. In contrast to that, at $V \approx 4$ kV the jet becomes suddenly shorter and less intense (see middle part of Fig. 3), but with a further increase of the applied voltage its length and brightness continuously rises again (Fig. 3, lower part).

The simultaneously recorded voltage and current signals are shown in Fig. 4. In all presented cases the strong spikes are present in current signals (U_1) which are due to coupling of the function generator and the high-voltage plasma generator to the oscilloscope input. This can be clearly seen in the upper part of Fig. 4 on the left side, where the output of the high-voltage plasma generator was set to zero. The separation between these spikes ($23 \mu\text{s}$) represents the half-periods of the applied rectangular input signal (21.5 kHz).

When the voltages up to 4 kV are applied, near each high spike there is an additional peak, which represents the plasma ignition. In Fig. 4 these peaks are indicated by open arrows. The width of these peaks which is less than $2 \mu\text{s}$, which cannot be discerned in the figure, corresponds to the time when the plasma is on. At voltages higher

than 4 kV, the current signals show additional randomly distributed current peaks. In Fig. 4 the positions of these random peaks are indicated by full arrows. With increasing voltage, these randomly distributed peaks become more pronounced, which is illustrated for the applied voltage of 6.0 kV in the right lower part of Fig. 4. Nevertheless, the sharp peaks appearing at voltages below 4 kV (marked with open arrows) are still present also at higher voltages.

Wagner et al. [24] showed that DBDs can work in different modes, which can be generated under special conditions. They discussed the physical properties and the main electrical parameters, which are necessary for controlled DBD operations. When a sharp single current peak appears the plasma operates in a homogeneous mode, while randomly distributed current peaks can be observed when the plasma is in a filamentary mode. Following the findings of Wagner et al. [24], we conclude that our present capillary DBD is running in the homogeneous mode at voltages below 4 kV, while at higher voltages it is characterized mainly by the filamentary mode operation.

3.2. Emission intensity distributions

During the experiments using the plasma jet as soft ionization source it was observed that a slight change of the applied voltage could change the mass spectrometric signal by two orders of magnitude. The measurements turned out that neither high flow rates nor high applied voltages will increase the efficiency of soft ionization. To get a better insight in the relevant processes, the spatial distributions of excited helium atoms and N_2 and N_2^+ molecules were investigated by measuring the corresponding emission intensities along the discharge axis x for various discharge voltages and helium gas flows. The applied voltage range was between 3 and 6.5 kV, while the chosen He flow rates were 250, 500 and 1000 ml/min.

As for the excited He atoms, in the present case there are six lines (at 388, 501, 587, 667, 706 and 728 nm) at disposal in UV and visible region. These lines correspond to the transitions from higher excited states to either $2p \ ^1P_1^o$ resonance state or the lower-lying $2p \ ^3P_{2,1,0}^o$ as well as the metastable $2s \ ^1S_0$ and the $2s \ ^3S_1$ states. Here we present the results obtained for the He 388 nm line (see Fig. 5), which occurs in transition between the $3p \ ^3P_0^o$ state and the lowest metastable $2s \ ^3S_1$ state.

The spatial intensity distributions of all other He lines (not shown here) were found to be very similar mutually, and each of them can be regarded as a good indicator of distributions of the excited helium atoms. For the sake of simplicity, the He 388 nm line was chosen as

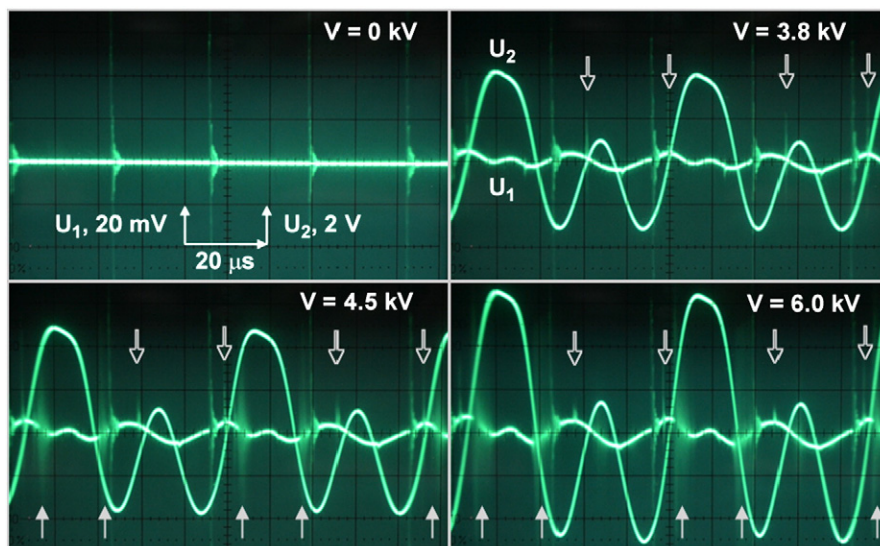


Fig. 4. Voltage (U_2) and current (U_1) signals. See further explanations in text. The numbers (in kV) represent voltage amplitude, while its peak-to-peak value is captured on the photographs.

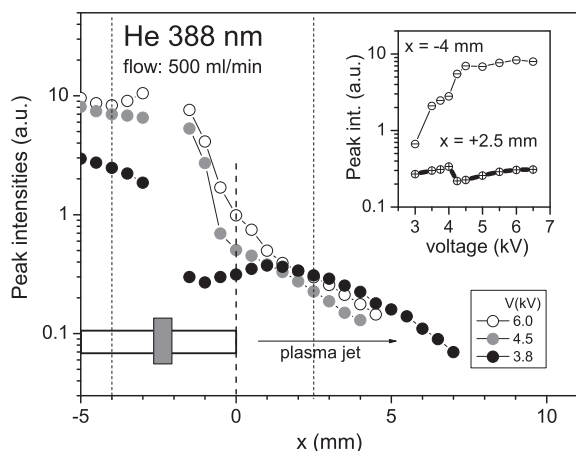


Fig. 5. Spatial distribution of the peak-intensity of the He 388 nm line measured at three different voltages at He flow of 500 ml/min. Inset: Voltage-dependent intensities of the He 388 nm line measured in the capillary near the anode ($x = -4$ mm) and in the jet ($x = +2.5$ mm). The experimental error bars are of the size of the symbols.

the most appropriate representative because in the spectrum it lays close to the measured N_2 and N_2^+ molecular bands. The He 388 nm line intensity distribution was measured along the x-axis starting from a position in the capillary between the electrodes. The position of the anode around the capillary tube is marked by a gray rectangle. The open end of the capillary is indicated by a dashed line and chosen as the zero-position.

In Fig. 5 the peak line intensity distributions of the He 388 nm line are displayed. The spatial distributions along the x-axis were measured for three characteristic discharge voltages at a constant He flow (500 ml/min). The He 388 nm line intensities in the jet are generally much lower than those in the capillary. However, the intensities in the capillary and in the jet exhibit quite different dependence on the applied voltage, which is presented in more detail in the inset of Fig. 5. The peak intensity of the He 388 nm line measured at a fixed position in the capillary ($x = -4$ mm) rises up for about one order of magnitude while increasing the voltage from 3 kV to 6.5 kV, whereas an inflection at about 4 kV occurs. In contrast to that, the intensities in the jet ($x = +2.5$ mm) first increase in the region between 3 kV and 4 kV. At latter voltage the intensities show a significant drop and by further raise of the voltage show smooth increase again. The present measurements show that the excited helium atoms extend farthest in the plasma jet for the applied voltage just below a critical value of 4 kV. This is in accordance with qualitative results presented in the previous section. It should be stressed that at that point the consumed discharge power amounts only about 30% of the power related to the maximum applied voltage.

Analogous to the case of the He 388 nm line, the intensity distributions of the heads of the N_2^+ 391 nm and N_2 380 nm bands are given in Figs. 6 and 7, respectively. In the present case, the partial density of N_2 for $x \leq 0$ is constant and amounts to about 3 ppm (used working gas: He 5.0), while for $x > 0$ it rises to the ambient air value in the way which is determined by the applied He flow. On the other hand, the excited nitrogen ions and neutrals outside of the capillary are produced due to collisions with either excited or charged particles leaving the discharge region. Therefore, as one can see in Figs. 6 and 7, the maxima of the excited N_2^+ and N_2 in the plasma jet occur at a certain distance from the capillary outlet. In the filamentary mode, i.e. at voltages higher than 4 kV, these maxima are closer to the capillary outlet than in the case of a homogeneous discharge mode. Maximum production of N_2^+ in the plasma jet occurs in the homogeneous mode at voltages close to the critical point (4 kV), which is illustrated by the distribution obtained at

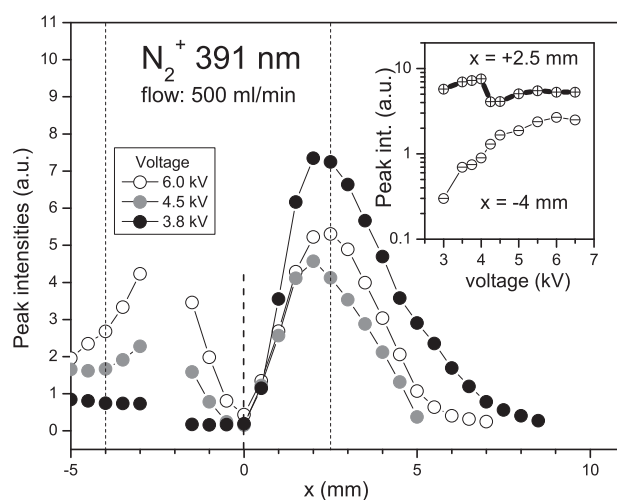


Fig. 6. Spatial distribution of the head of the N_2^+ 391 nm band measured at three different voltages at He flow of 500 ml/min. Inset: Voltage-dependent intensities of the N_2^+ 391 nm band measured in the capillary near the anode ($x = -4$ mm) and in the jet ($x = +2.5$ mm). The experimental error bars are of the size of the symbols.

3.8 kV as shown in Fig. 6. As one can see in Fig. 7, in that case the maximum of the N_2 380 nm signal compared with the maximum of the N_2^+ 391 nm signal (see Fig. 6) has a shift in the direction away from the outlet. Otherwise, no corresponding shift can be determined for the cases when higher voltages were applied.

The comparison of the insets in Figs. 5 and 6 reveals that the voltage-dependent intensities of the He 388 nm line and the N_2^+ 391 nm band measured at fixed x-positions in the capillary and in the jet are of similar shape. However, in contrast to the He 388 nm line, the voltage-dependent intensity of the N_2^+ 391 nm band near the anode ($x = -4$ mm) is generally much smaller than in the jet at the position of the maximum ($x = +2.5$ mm).

The voltage-dependent intensities of the N_2 380 nm band in the jet show similar dependence as those of the He 388 and N_2^+ 391. They raise monotonously with increasing voltage up to 4 kV, where a clear drop occurs after which they continue to increase again. However, inside the capillary near the anode, the N_2 380 nm band intensity changes

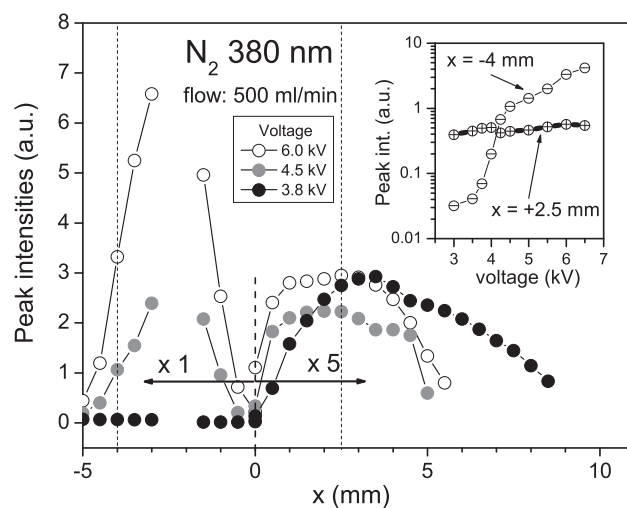


Fig. 7. Spatial distribution of the head of the N_2 380 nm band measured at three different voltages at He flow of 500 ml/min. Inset: Voltage-dependent intensities of the N_2 380 nm band measured in the capillary near the anode ($x = -4$ mm) and in the jet ($x = +2.5$ mm). The experimental error bars are of the size of the symbols.

for about two orders of magnitude for voltages ranging between 3.5 and 6 kV. The steepest intensity increase appears when the applied voltage approaches the critical value of 4 kV.

It should be stressed that the presented voltage dependences for all three cases are very reproducible and without hysteresis. The general reproducibility of the presented results was checked using four electrode sets and repeating the measurements several times for each individual setup. Nevertheless, the critical voltage is slightly different for various electrode sets of the same dimension and varies in the region between 3.8 kV and 4.3 kV. This is obviously due to the quality of established quartz–metal contacts in each particular case. As for the change of the applied gas flow, in the range from 250 ml/min to 1000 ml/min no influence on the value of the critical voltage was observed. However, as already shown in our previous work [20], the shapes of the intensity distributions are strongly affected by the applied helium flow. This is illustrated in Fig. 8 where the previously presented peak intensity x -distributions of He 388 nm, N_2^+ 391 nm and N_2 380 nm obtained in a homogeneous mode at the voltage of 3.8 kV and the flow of 500 ml/min are compared with the data obtained for the same voltage at a lower (250 ml/min) and a higher He flow (1000 ml/min).

The measured intensities in the anode region and in the jet become stronger while increasing the gas flow. Simultaneously, the widths of their distributions in the jet become longer and are shifted away from the capillary outlet. This is due to the fact that with the increasing flow the distributions of the excited species in the capillary become asymmetric. When looking at the line intensity distributions in the whole region between the electrodes (not shown here) they exhibit nearly symmetric shapes for helium flows up to about 200 ml/min. When the flow increases, the intensities in the region of the inner electrode (cathode) become smaller, while in the anode region and in the jet they become stronger. Since the density of N_2^+ is crucial for water protonation and soft ionization, according to the results presented in Fig. 8 (see upper part on the right side of the figure) one could make a straightforward conclusion that the highest gas flows lead to the most efficient soft ionization. Nevertheless, high flows of working gas can affect the density of probed species in the reaction chamber, so that an optimum of soft ionization should be expected at some compromise conditions, i.e. at moderate gas flows.

3.3. Distributions of N_2^+ rotational temperatures

From the measurements performed in the present experiment one can deduce the information about the rotational temperatures

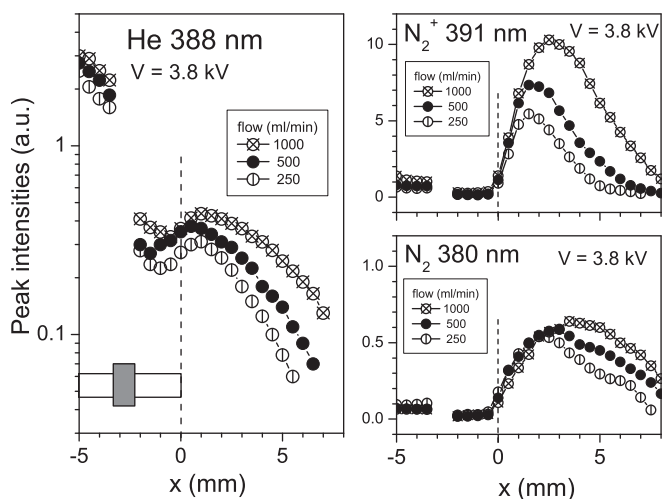


Fig. 8. Spatial distributions of the peak intensities of the He 388 nm line together with head intensity distributions of the N_2^+ 391 nm and N_2 380 nm bands measured in a homogeneous mode at various helium flows.

of the N_2^+ molecule using the line intensities of the N_2^+ band with maximum at 391 nm. Molecular rotational temperature is the excitation temperature obtained from the Boltzmann plot involving the populations in relevant rotational states and represents an important element in plasma diagnostics. Because of rapid collisional establishment of equilibrium between rotational and translational energies, the rotational temperatures are commonly accepted as a reliable indicator for the gas temperatures. For example, the spectra in the region between the He 388 nm line and the head of the N_2^+ 391 band recorded for two extreme cases are plotted in Fig. 9. In the first case, the spectrum was measured in the capillary at position $x = -6$ mm. In that case the applied voltage was 3.8 kV and the DBD was running in the homogeneous mode. In the second case the spectrum was measured in the jet at $x = +2$ mm, whereas the DBD was running in a filamentary mode at 6.5 kV.

The molecular lines in Fig. 9 are labeled with quantum numbers K'' belonging to the corresponding lower rotational levels. In general, the population of excited states n_i of a quantum system in equilibrium is described by Boltzmann distribution $n_i \propto g_i \exp(-E_i/kT)$, where g_i and E_i are statistical weight and the energy of the i -th level, respectively, while k and T label the Boltzmann constant and the excitation temperature. By measuring the intensities $I_{ik} \propto (1/\lambda_{ik}) n_i A_{ik}$ of the optically thin lines (λ_{ik} : line wavelength, A_{ik} : line transition probability) in the transition $i \rightarrow k$, the excitation temperatures can be evaluated from the Boltzmann plot, i.e. from the linear relationship between the data $\ln(\lambda_{ik} I_{ik}/g_{ik} A_{ik})$ and E_i/kT . The rotational excitation temperatures for the N_2^+ band measured here were determined using the relative intensities $I(K'')$ of eleven marked lines (from $K'' = 6$ to $K'' = 16$, see Fig. 9). Following the expressions taken from reference [25], the calculated values of $\log [I(K'') c / (2(K'' + 1))]$ were plotted against the values $(K'' + 1)(K'' + 2)$. Here, the factor c amounts to 1 or 2 for even and odd values of quantum numbers K'' , respectively. Then, the rotational temperature T_{rot} (K) can be evaluated from the slope s of this linear relationship, which equals to $-1.296/T$.

For the present examples (see inset of Fig. 9) the Boltzmann plots exhibit clear differences in the slopes. In the first case the slope $s_c = -0.000312$, while in the second case $s_j = -0.000384$. With the statistical errors as well as the uncertainties in measured signals included, the calculated rotational temperatures in the capillary at

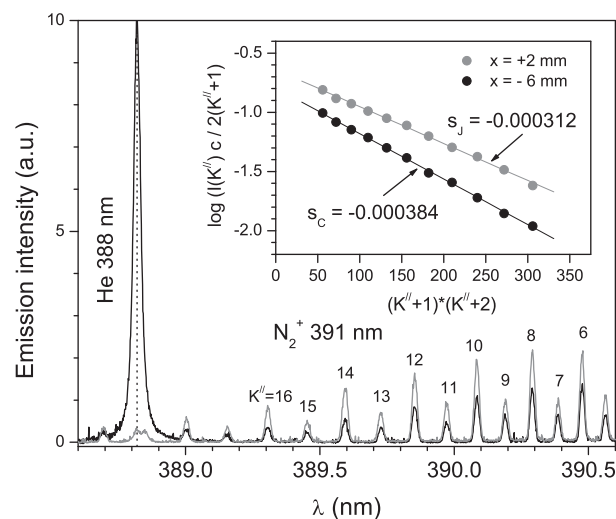


Fig. 9. The emission spectra of the He 388 nm line and the part of the N_2^+ 391 band measured in a homogeneous mode ($V = 3.8$ kV) in the capillary (black line) and in a filamentary mode ($V = 6.5$ kV) in the jet (gray line). The measurements were performed at the helium flow of 500 ml/min. The numbers K'' attributed to the particular molecular lines are the rotational quantum numbers of the corresponding lower level in the $N_2^+(B^2\Sigma_u^+ \rightarrow N_2^+(X^2\Sigma_u^+))$ transitions. Inset: The Boltzmann plots constructed by using the intensities of eleven marked (from $K'' = 6$ to $K'' = 16$) molecular lines. See further explanation in text.

$V = 3.8$ kV and in the jet at $V = 6.5$ kV amount to (337 ± 8) K and (415 ± 10) K, respectively.

The examples presented in Fig. 9 are a part of the measurements of the spatial distributions of rotational temperatures at He flow of 500 ml/min, the final results of which are plotted in Fig. 10 (left). Here, the measurements of rotational temperatures in both homogeneous and filamentary mode were performed along the discharge axis from the middle of the capillary to the positions in the jet where the lines of the N_2^+ 391 band are still measurable. As shown in Fig. 10, for the DBD operating in the filamentary mode, the rotational temperatures are practically the same (about 40 K above the room temperature). In the filamentary mode there is a clear increase of rotational temperatures when approaching the anode region and their values saturate in the jet at about 410 K. The influence of applied voltages and He flows on rotational temperatures is illustrated in the right part of Fig. 10.

Generally, with increasing the helium flow, the rotational temperatures are lowered, which is plausible since in that case the cooling of the discharge due to convection is more efficient. Up to the critical voltage of about 4 kV, the rotational temperatures at a given helium flow remain constant. At voltages above the critical value, the rotational temperatures exhibit a monotonous increase so that at highest voltages applied in the present experiment the rotational temperatures are more than 100 K above the room temperature. As presented in the next section, this significant change of the rotational temperatures leads to important conclusions about the formation of N_2^+ under the present experimental conditions.

4. Discussions

The ground state of the nitrogen ion molecule N_2^+ ($X^2\Sigma_g^+$) is commonly regarded as crucial particle for water dissociation and soft ionization in atmospheric plasmas. Under the conditions in the present experiment, the population of the state N_2^+ ($X^2\Sigma_g^+$) in the plasma jet is directly dependent on the transition N_2^+ ($B^2\Sigma_u^+$) \rightarrow N_2^+ ($X^2\Sigma_g^+$) in which the N_2^+ 391 nm band occurs. Therefore, the intensity of the N_2^+ 391 nm band in the jet is an important factor for estimating the efficiency of soft ionization.

4.1. Discussion on excitation of N_2^+ and N_2

In contrast to helium-based discharges, the N_2^+ 391 nm emission cannot be initiated in pure nitrogen DBD plasmas at atmospheric air

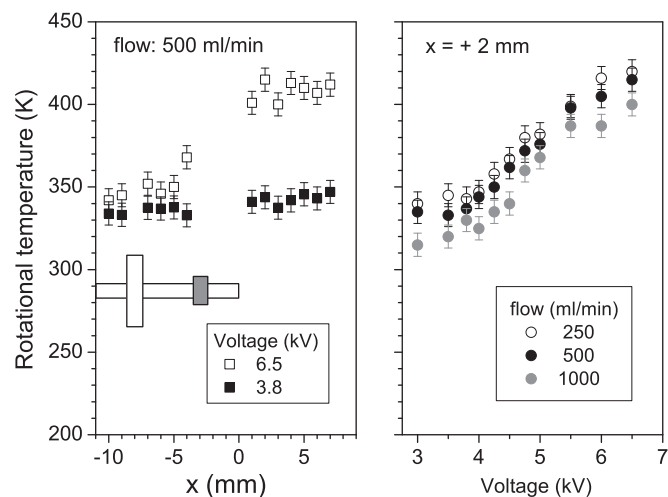
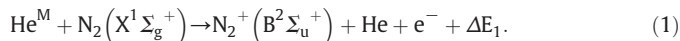


Fig. 10. Left: Spatial distributions of the N_2^+ rotational temperatures measured at constant helium flow (500 ml/min) in the homogeneous (black squares) and in the filamentary mode (open squares). Right: The dependence of N_2^+ rotational temperatures on the applied voltage measured at fixed position in the plasma jet for three different He flows.

[23,26]. In helium-based DBD discharges the N_2^+ ($B^2\Sigma_u^+$) state could be in principle populated either due to electron impact or due to energy transfer in collisions with highly excited helium species. As for the collisions with electrons this state could be possibly populated through two different processes. The first process is the one-step electron impact ionization process: N_2 ($X^1\Sigma_g^+$) $_{v=0} + e^-$ ($E > 18.7$ eV) \rightarrow N_2^+ ($B^2\Sigma_u^+$) $_{v=0} + 2e^-$. The second one is the two-step process: N_2 ($X^1\Sigma_g^+$) $_{v=0} + e^-$ ($E > 15.5$ eV) \rightarrow N_2^+ ($X^2\Sigma_g^+$) $_{v=0} + 2e^-$ followed by: N_2^+ ($X^2\Sigma_g^+$) $_{v=0} + e^-$ ($E > 3.2$ eV) \rightarrow N_2^+ ($B^2\Sigma_u^+$) $_{v=0} + e^-$. These processes probably could take place during the initial increase and the early decay of the current pulse when the density of fast electrons inside the capillary is high.

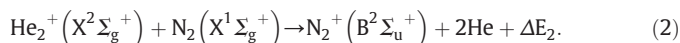
However, one should keep in mind that the DBD burns in a relatively short period of time, in the present experiment less than 2 μ s, and in the relatively long period of time between two discharge pulses there are no fast electrons present. In addition, the formation of N_2^+ in the plasma jet and a significant increase of N_2^+ 391 band intensity at lower voltages cannot be explained by electron impact.

It is commonly accepted that the process of N_2^+ formation in helium-based atmospheric plasmas is initiated by highly excited helium species, i.e. excited helium atoms (He^* , including helium metastables He^M) and ions (He^+ , He_2^+). As shown by time-resolved measurements reported by Xiong et al. [21], the excited N_2^+ are present in this “dark” period between two discharge pulses when plasma is generated in helium. As pointed out in that work, this is most probably due to Penning ionization involving the helium metastables and ground-state nitrogen molecules:



The helium metastables are created in the short pulse periods in between the electrodes and their effective lifetime in the later phases is governed by collisions with air components.

As an alternative path for the formation of ionized nitrogen molecules (see for instance [18] and references therein), the charge transfer in collision with ground-state helium ion dimers and nitrogen molecules is proposed:



Both (1) and (2) collisional excitation energy transfer (CEET) reactions are exothermic, whereas the energy defect in the case of CT is significantly higher than in the case of PI. For instance, in the case of lowest lying helium metastables He^M ($2s^3S_1$) the energy defect $\Delta E_1 = 6650$ cm^{-1} , while the energy ΔE_2 in the reaction (2) amounts to 25,770 cm^{-1} .

The helium dimer ion He_2^+ can be formed in several ways and in atmospheric plasmas the most effective process is the three-body association $He^+ + 2He \rightarrow He_2^+ + He$. The He_2^+ is a relatively stable molecule and, as pointed out in [18], it is generally agreed that He_2^+ is dominant and of greater population density than the helium atomic ions He^+ in discharges operating at pressures higher than several tens of mbar.

The paths leading to the population of relevant excited states have been discussed and proposed in [10]. The N_2 emissions at 380 nm correspond to the transition N_2 ($C^3\Pi_u^+$) \rightarrow N_2 ($B^3\Pi_g^+$). The N_2 ($C^3\Pi_u^+$) state can be populated in several ways. First, it can be populated through the direct electron impact excitation from the N_2 ground state: N_2 ($X^1\Sigma_g^+$) $_{v=0} + e_{fast}^- \rightarrow N_2$ ($C^3\Pi_u^+$) $_{v=0,1} + e_{slow}^-$, where the threshold energy of fast electrons equals to 11.1 eV. In this case, the population rate for the upper level of the N_2 transition at 380 nm is proportional to the N_2 ground state number density and the density of fast electrons. A second possible population mechanism of the N_2 ($C^3\Pi_u^+$) state is through electron recombination of the N_2^+ ($X^2\Sigma_g^+$) followed by decay. Since the electron density in the vicinity of the anode increases with higher applied voltage, the electron recombination rate

of the N_2^+ ($X^2\Sigma_g^+$) increases too, and can produce an additional density increase of the N_2 ($B^3\Pi_g^+$). This can be seen in the inset of Fig. 7, which shows a strong increase of the peak intensity of the N_2 380 nm band measured near the anode while the increasing discharge voltage approaches the critical value of about 4 kV.

4.2. Discussion on intensity distributions

The emission molecular bands measured side-on in the present experiment were optically thin and therefore they can be directly correlated with the corresponding number densities of excited helium atoms and N_2 and N_2^+ molecules. Without going into the details here, the optical thickness of the side-on measured spectral features was checked by comparison with end-on measured signals, i.e. with the emission from about 20 times longer plasma layer. Therefore, the relative intensities of measured bandheads yield the information about the relative populations in the excited states of relevant species. An additional insight in the excitation and de-excitation processes under the present experimental conditions can be obtained from the peak intensity ratios $I(391)/I(380)$ of the N_2^+ 391 nm and N_2 380 nm bands. This ratio is directly proportional to the ratio of the population densities in N_2^+ ($B^2\Sigma_u^+$) and N_2 ($C^3\Pi_u^+$). According to the above considerations, the ground state number density of N_2^+ in the plasma jet can be regarded to be proportional to the density in the N_2^+ ($B^2\Sigma_u^+$) state. Thus, the ratio $I(391)/I(380)$ can be regarded as proportional to the N_2^+ ($X^2\Sigma_g^+$) to N_2 ($C^3\Pi_u^+$) density ratio too. Radiative and non-radiative de-activation of N_2^+ leading to formation of excited neutral nitrogen molecule are the processes which are competitive to the reactions in which N_2^+ ($X^2\Sigma_g^+$) acts as the source for water dissociation and soft ionization in atmospheric plasmas. Consequently, one can consider the higher values of peak intensity ratios $I(391)/I(380)$ as an indicator for higher probability of soft ionization.

In Fig. 11 the peak intensity ratios $I(391)/I(380)$ along the discharge axis are plotted. Here, the intensity ratios for three voltages ($V = 3.8$ kV, 4.5 kV and 6.0 kV) are obtained using the data for peak intensities presented in Figs. 6 and 7. Additional data, not previously presented, which were measured in the homogeneous mode at $V = 3.0$ kV and in the filamentary mode at $V = 5.0$ kV, are plotted too. The values for the ratios $I(391)/I(380)$ are clearly separated in two groups belonging to homogeneous and filamentary

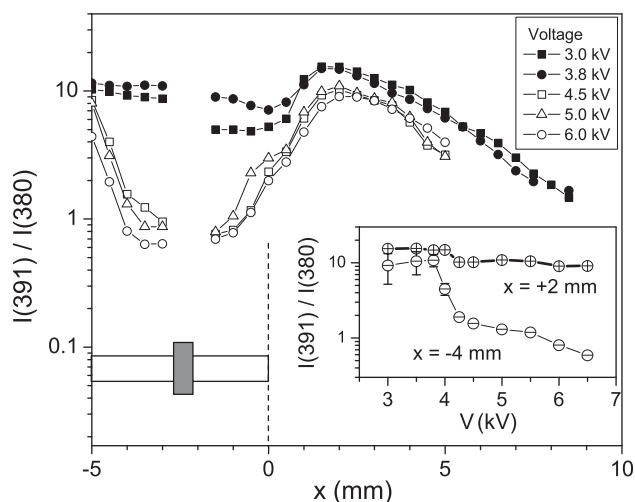


Fig. 11. Spatial distributions of peak intensity ratios $I(391)/I(380)$ for the N_2^+ 391 and N_2 380 nm bands at five various applied voltages. Inset: The values for $I(391)/I(380)$ measured in dependence on the applied voltage at fixed position near the anode ($x = -4$ mm) and in the jet ($x = +2$ mm). All data are related to the helium flow of 500 ml/min. With exception of first four points for $x = +2$ mm in the inset, the error bars are of the size of the used symbols. For the sake of picture clarity, the error bars related to x -distributions (about 30% for $x \geq 3$ mm) are omitted.

modes. In the anode region where the amount of N_2 in helium is small and constant, the $I(391)/I(380)$ ratio is about one order of magnitude smaller in the filamentary modes than in the homogeneous modes. As one can see in the inset of Fig. 11, there is a pronounced drop in the vicinity of the critical voltage $V = 4$ kV, which is presumably correlated with an increasing population in the N_2 ($C^3\Pi_u^+$) due to increasing recombination and electron-impact processes. The data in Fig. 11 show that the intensity ratio $I(391)/I(380)$ in the plasma jet is about 2 times higher in the homogeneous mode operation than in the case of filamentary modes. Independent of the applied voltage, the maximum of the $I(391)/I(380)$ ratio occurs at distances between 1.5 and 2 mm away from the capillary end. This fact, combined with the previously presented maxima of N_2^+ 391 intensity distributions (Fig. 6), leads to the conclusion that an optimum of soft ionization under the present experimental conditions can be expected at the distance of about 2 mm from the capillary edge and with the DBD operating in the homogeneous mode just below the critical voltage.

4.3. Discussion on rotational temperature distributions

When judging which of the two above mentioned CEET processes is dominant in formation of N_2^+ and, consequently, more important for soft ionization under the present experimental conditions, the results presented previously in Section 3.3 can be very helpful and instructive. In the case of DBD operating in a homogeneous mode, the rotational N_2^+ temperatures are slightly above the room temperature in the capillary as well as in the plasma jet, which should be related with the excitation pathway (1) for the production of N_2^+ . Namely, as reported in [27,28], the rotational temperatures of N_2^+ ($B^2\Sigma_u^+$) produced in PI reaction (1) are only few tens of Kelvin degrees higher than the ambient temperature. In contrast to that, the CT reaction (2) yields the N_2^+ ($B^2\Sigma_u^+$) with rotational temperatures of about 900 K [28,29]. According to findings reported in [29], the corresponding Boltzmann plot is not linear, i.e. the higher rotational levels of N_2^+ ($B^2\Sigma_u^+$) formed in reaction (2) are overpopulated and exhibit smaller slope than the lower lying rotational levels. An interesting behavior of N_2^+ ($B^2\Sigma_u^+$) rotational temperatures is reported in Ref. [18]. Similar to the case of the present DBD operating in the filamentary mode, the spatial distributions of N_2^+ ($B^2\Sigma_u^+$) rotational temperatures in the plasma jet produced by a DBD in [18] show an increase at larger distances from the plasma origin. In contrast to the present results, this increase is monotonic and does not exhibit saturation. The temperatures at largest considered distances rise up to 550 K. The conditions here and in [18] are certainly not the same. For instance, the gas velocities in the present experiment are about one order of magnitude higher. In addition, the discharge tube geometry as well as the electrode design is different. However, on the basis of the rotational temperature data, one can conclude that in the filamentary mode operation here and in the experiment reported in [18], the charge transfer reaction (2) in the plasma jet plays a significant role. Additional important finding in [18] is the fact that the simultaneously measured rotational temperatures of the OH molecule in the discharge and in the plasma jet are constant and lie in the range of 280 to 300 K. As concluded in [18], the common assumption that a rapid equilibrium exists between rotational levels and translation energies of a molecule in atmospheric-pressure plasma, is not fulfilled in the case of N_2^+ . Rotational temperatures of N_2^+ in helium based plasmas are not reliable measure of gas temperatures but rather an indicator of the of N_2^+ reaction channel production.

According to the results obtained here for the increased rotational temperatures of N_2^+ , it can be concluded that under the present experimental conditions, the formation of N_2^+ ions in the plasma jet produced by the DBD running at high voltages in filamentary mode is due to comparable contributions of both reactions (1) and (2). This conclusion is justified because in such mixed case the expected rotational temperatures should be between 300 and 900 K. On the other hand,

when the present DBD is running at lower voltages, i.e. in the homogeneous mode, the rotational temperatures are close to room temperature and the major production of N_2^+ should be attributed to the Penning ionization process (1).

5. Conclusions

The plasma properties affected by the discharge modes are very important for a better understanding of the ionization process in DBDs. The experiments presented here point out that the plasma jet can operate in two different voltage depending modes. These are homogeneous and filamentary modes, which can be recognized visually monitoring the plasma appearance and simultaneously inspecting the measured plasma current. Filamentary modes show multiple current peaks while a homogeneous mode has a well-defined current peak. For soft ionization with less fragmentation of molecules the plasma jet should be driven in a homogeneous mode. When the plasma jet is adjusted to its longest extension, while working in a homogeneous mode, most of the energy will be coupled into the jet. Under these conditions the biggest separation of the N_2^+ and the N_2 maxima can be observed and the most efficient soft ionization can be expected. In that case, the major production of N_2^+ in the plasma jet is due to the helium metastable atoms.

First measurements with the plasma jet as a dielectric barrier discharge based ambient ionization (DBDI) were already performed in our group [30]. Measurements of an Ar-DBDI, entirely filamentary discharge, were compared with two homogeneous discharges, a He-DBDI and an Ar/ NH_3 -DBDI, all three with the same configuration. As a clear outcome, filamentary Ar-DBDI reveals only poor ionization efficiency with a drastic increase of analyte fragmentation compared to homogeneous He-DBDI and Ar/ NH_3 -DBDI, respectively.

Our further measurements with the plasma jet will be focused on the determination of the density of the He metastable atoms and thereby on the soft ionization mechanism to increase the MS-signal.

Acknowledgments

Financial support by the Ministerium für Innovation, Wissenschaft und Forschung des Landes Nordrhein-Westfalen, the Bundesministerium für Bildung und Forschung, the Deutsche Forschungsgemeinschaft (DFG) and the Ministry of Science, Education and Sports of the Republic of Croatia (project No. 035-0352851-2853) is gratefully acknowledged.

References

- [1] N. Na, M. Zhao, S. Zhang, C. Yang, X. Zhang, Development of a dielectric barrier discharge ion source for ambient mass spectrometry, *J. Am. Soc. Mass Spectrom.* 18 (2007) 1859–1862.
- [2] J.D. Harper, N.A. Charipar, C.C. Mulligan, X. Zhang, R.G. Cooks, Z. Ouyang, Low-temperature plasma probe for ambient desorption ionization, *Anal. Chem.* 80 (2008) 9097–9104.
- [3] J.S. Wiley, J.F. Garcia-Reyes, J.D. Harper, N.A. Charipar, Z. Ouyang, R.G. Cooks, Screening of agrochemicals in foodstuffs using low-temperature plasma (LTP) ambient ionization mass spectrometry, *Analyst* 135 (2010) 971–979.
- [4] A.U. Jackson, T. Shum, E. Sokol, A. Dill, R.G. Cooks, Enhanced detection of olefins using ambient ionization mass spectrometry: Ag⁺ adducts of biologically relevant alkenes, *Anal. Bioanal. Chem.* 399 (2011) 367–376.
- [5] M.Z. Huang, S.S. Jhang, C.N. Cheng, S.C. Cheng, J. Shiea, Effects of matrix, electrospray solution, and laser light on the desorption and ionization mechanisms in electrospray-assisted laser desorption ionization mass spectrometry, *Analyst* 135 (2010) 759–766.
- [6] Y. Zhang, X.X. Ma, S.C. Zhang, C.D. Yang, Z. Ouyang, X.R. Zhang, Direct detection of explosives on solid surfaces by low temperature plasma desorption mass spectrometry, *Analyst* 134 (2009) 176–181.
- [7] Y.Y. Liu, Z.Q. Lin, S.C. Zhang, C.D. Yang, X.R. Zhang, Rapid screening of active ingredients in drugs by mass spectrometry with low-temperature plasma probe, *Anal. Bioanal. Chem.* 395 (2009) 591–599.
- [8] A. Michels, S. Tombrink, W. Vautz, M. Miclea, J. Franzke, Spectroscopic characterization of a microplasma used as ionization source for ion mobility spectrometry, *Spectrochim. Acta B* 62 (2007) 1208–1215.
- [9] W. Vautz, A. Michels, J. Franzke, Micro-plasma: a novel ionisation source for ion mobility spectrometry, *Anal. Bioanal. Chem.* 391 (2008) 2609–2615.
- [10] S.B. Olenici-Craciunescu, A. Michels, C. Meyer, R. Heming, S. Tombrink, W. Vautz, J. Franzke, Characterization of a capillary dielectric barrier plasma jet for use as a soft ionization source by optical emission and ion mobility spectrometry, *Spectrochim. Acta B* 64 (2009) 1253–1258.
- [11] H. Hayen, A. Michels, J. Franzke, Dielectric barrier discharge ionization for liquid chromatography/mass spectrometry, *Anal. Chem.* 81 (2009) 10239–10245.
- [12] J.T. Shelley, G.M. Hieftje, Ionization matrix effects in plasma-based ambient mass spectrometry sources, *J. Anal. At. Spectrom.* 25 (2010) 345–350.
- [13] I. Dzidic, D.I. Carroll, R.N. Stillwell, E.C. Horning, Comparison of positive-ions formed in nickel-63 and corona discharge ion sources using nitrogen, argon, isobutane, ammonia and nitric oxide as reagents in atmospheric pressure ionization mass spectrometry, *Anal. Chem.* 48 (1976) 1763–1768.
- [14] A. Ricard, P. Decomps, F. Massines, Kinetics of radiative species in helium pulsed discharge at atmospheric pressure, *Surf. Coat. Technol.* 112 (1999) 1–4.
- [15] F. Massines, P. Segur, N. Gherardi, C. Khamphan, A. Ricard, Physics and chemistry in a glow dielectric barrier discharge at atmospheric pressure: diagnostics and modelling, *Surf. Coat. Technol.* 174 (2003) 8–14.
- [16] C. Anderson, M. Hur, P. Zhang, L. Mangolini, U. Kortshagen, Two-dimensional space-time-resolved emission spectroscopy on atmospheric pressure glows in helium with impurities, *J. Appl. Phys.* 96 (2004) 1835–1839.
- [17] W.C. Zhu, Q. Li, X.M. Zhu, Y.K. Pu, Characteristics of atmospheric pressure plasma jets emerging into ambient air and helium, *J. Phys. D: Appl. Phys.* 42 (2009).
- [18] G.C.Y. Chan, J.T. Shelley, J.S. Wiley, C. Engelhard, A.U. Jackson, R.G. Cooks, G.M. Hieftje, Elucidation of reaction mechanisms responsible for afterglow and reagent-ion formation in the low-temperature plasma probe ambient ionization source, *Anal. Chem.* 83 (2011) 3675–3686.
- [19] T. Martens, D. Mihailova, J. van Dijk, A. Bogaerts, Theoretical characterization of an atmospheric pressure glow discharge used for analytical spectrometry, *Anal. Chem.* 81 (2009) 9096–9108.
- [20] S.B. Olenici-Craciunescu, S. Mueller, A. Michels, V. Horvatic, C. Vadla, J. Franzke, Spatially resolved spectroscopic measurements of a dielectric barrier discharge plasma jet applicable for soft ionization, *Spectrochim. Acta B* 66 (2011) 268–273.
- [21] Q. Xiong, X. Lu, J. Liu, Y. Xian, Z. Xiong, F. Zou, C. Zou, W. Gong, J. Hu, K. Chen, X. Pei, Z. Jiang, Y. Pan, Temporal and spatial resolved optical emission behaviors of a cold atmospheric pressure plasma jet, *J. Appl. Phys.* 106 (2009).
- [22] Z. Xing, J.A. Wang, G.J. Han, B. Kuermaiti, S.C. Zhang, X.R. Zhang, Depth profiling of nanometer coatings by low temperature plasma probe combined with inductively coupled plasma mass spectrometry, *Anal. Chem.* 82 (2010) 5872–5877.
- [23] R. Heming, A. Michels, S.B. Olenici, S. Tombrink, J. Franzke, Electrical generators driving microhollow and dielectric barrier discharges applied for analytical chemistry, *Anal. Bioanal. Chem.* 395 (2009) 611–618.
- [24] H.E. Wagner, R. Brandenburg, K.V. Kozlov, A. Sonnenfeld, P. Michel, J.F. Behnke, The barrier discharge: basic properties and applications to surface treatment, *Vacuum* 71 (2003) 417–436.
- [25] P.W.J.M. Boumans, Inductively coupled plasma emission spectroscopy, Part II: *Appl. fundam.* 2 (1987).
- [26] A. Qayyum, S. Zeb, M.A. Naveed, S.A. Ghauri, M. Zakaullah, A. Waheed, Diagnostics of nitrogen plasma by trace rare-gas-optical emission spectroscopy, *J. Appl. Phys.* 98 (2005).
- [27] W.C. Richards, D.W. Setser, Penning ionization optical spectroscopy: metastable helium (He 2 S) atoms with nitrogen, carbon monoxide, oxygen, hydrogen chloride, hydrogen bromide, and chlorine, *J. Chem. Phys.* 58 (1973) 1809–1825.
- [28] M. Endoh, M. Tsuji, Y. Nishimura, Thermal energy charge-transfer reactions – He2(+) with N2 and CO, *J. Chem. Phys.* 79 (1983) 5368–5375.
- [29] A.E. Belikov, Rotational and vibrational excitation of the N2+ (B) state in a He + N2 electron-beam plasma, *Chem. Phys.* 215 (1997) 97–109.
- [30] C. Meyer, S. Müller, B. Gilbert-Lopez, J. Franzke, Impact of homogeneous and filamentary discharge modes on the efficiency of plasma based ambient ionization mass spectrometry, *Anal. Bioanal. Chem.* 405 (2013) 4729–4735.